ICAST2014 #028

Additive Manufacturing of Active Struts for Piezoelectric Shunt Damping

Dirk Mayer[1,3], Hanns A. Stoffregen[2,3], Oliver Heuss[1,3], Jennifer Pöllmann[1,3], Eberhard Abele[2,3], Tobias Melz[1,3]

[1] Fraunhofer Institute for Structural Durability and System Reliability (LBF), Darmstadt, Germany
[2] Institute of Production Management, Technology, and Machine Tools (PTW), Technische Universität Darmstadt, Darmstadt, Germany
[3] LOEWE Research Center AdRIA, Darmstadt, Germany

Abstract

Nowadays a lot of structures, like ships, aircrafts, wind turbines and engines are designed as lightweight structures. They are susceptible to disturbances caused by vibrations and other mostly unwanted excitations. Hence the performance, lifetime and system behavior of the structures are negatively influenced. One strategy to overcome these drawbacks might be an integration of actuators in such a system. As smart devices piezoceramic multilayer actuators (MLA) can be used. They offer the possibility of high level system integration and can generate strong forces. For low-cost system control, semi-passive or -active techniques can be used. The performances of both strategies depend mainly on the ratio of energy which can be transformed from the mechanical structure into electrical circuits. The generalized electromechanical coupling coefficient, a common measure describing this energy transfer, is highly influenced by the host structure's stiffness or the housing. Thus, a flexible and adjustable manufacturing technology is needed to optimize this generalized coupling factor. Emerging additive manufacturing technologies such as selective laser melting (SLM) are capable of a cost-efficient production of individualized parts in rather small production runs and to meet the manufacturing constraints of highly integrated components. In the presented research work SLM is used to manufacture active struts by fully integrating MLA into a metallic, monolithic housing. Besides the fulfillment of associated manufacturing constraints (e.g. low volume, individualization), a major objective of this study is to demonstrate the potential of SLM for application tailored smart components. A six cell truss structure is used as demonstration platform. Based on the numerical simulation of the truss structure and the application of the elastic strain intensity criterion the positioning of the active strut as well as the mode to be damped are determined. A numerical implementation of the active strut, specifically the piezoceramic actuator and corresponding housing, allows the dimensioning of the housing stiffness using the generalized electromechanical coupling factor criterion and are a starting point in the design of a resistive resonant shunt (RL-shunt). Using the results from the numerical simulation active struts with specific stiffness characteristics are manufactured via SLM. An experimental modal analysis of the truss structure is carried out. Measurements with connected RL-shunts using the active struts are performed and compared to the passive system. Results indicate an efficient damping of the desired mode by means of application tailored active struts. In addition, a good accordance between simulation and experimental results is obtained. This allows rapid design and positioning of active struts and corresponding RL-shunts for future work.

1. INTRODUCTION

Vibration control has gained significant importance during the last decades to enable higher precision in manufacturing machinery, decrease fatigue loads on infrastructure or enhance comfort in automobiles. Especially lightweight structures are prone to vibration problems. Truss structures are typical examples for this type of structures; the basic design is applied in space structures, but also used in civil engineering like bridges, or for spaceframe structures of high performance cars.

Studies on passive tuned vibration absorbers [2, 3] or active inertial mass actuators [4] for truss structures have been conducted and proven their performance.

The application of materials like piezoceramics allows for the structural integration of vibration control systems, which seems an interesting alternative to established solutions, since no additional inertial mass is required. Piezoelectric transducers can also be used for semi-active or passive damping by using electrical shunt circuits, which minimizes the effort for additional components like sensors or control electronics [5]. This technique has already successfully been implemented several years ago for a laboratory truss structure with shunted piezoelectric struts [6]. Due to the brittle material characteristics and the need of a proper mechanical pre-stress the design of a piezoelectric strut includes a design of a parallel stiffness and a housing that prevents tensile or shear forces from the piezo actuator. In the past manufacturing and structural integration of piezoelectric structures has been studied mostly for CFRP structures [7, 8]. For a steel or aluminum truss, however, a way for actuator integration into metallic components is required. In past studies, integration of piezoelectric elements into high-pressure die cast structures or metal panels was analyzed [9, 10]. Those manufacturing technologies are aiming at a mass production, which is not applicable for many active systems. A technology for the flexible and fast integration of piezoelectric elements into metal structures would enable the implementation of small series of active systems for industrial applications of active or semi-active vibration control. To this end, in this paper the integration of additive manufacturing into the development of smart structures is studied in this paper. The rest of the paper includes an introduction into the manufacturing process of the piezoelectric strut, a brief overview of the demonstration structure, the applied methods for semi-active damping and finally the numerical and experimental results.

2. RESEARCH METHODOLOGY

2.1 Selective laser melting of active struts

Additive manufacturing (AM) is an emerging field in manufacturing technologies that has the common principle of building up solid parts directly from 3D CAD data by adding material layer by layer. Part-specific tools are not required in these technologies. Additive manufacturing technologies allow the generation of parts which fulfil the properties of final products [11–13]. Among AM technologies, selective laser melting (SLM) has become a relevant production method for manufacturing ready-to-use parts made from metals such as stainless steel, nickel, titanium, and aluminum alloys [14]. As AM technology SLM enables the following key advantages for innovative products: function optimized and application tailored product design, functional integration, mass customization, resource efficiency, and shortened time to market [15–17].

The fundamental process steps of the SLM technique are shown in Figure 1. A 3D CAD model (Step 1) of the part to be built is sliced in single layers (Step 2). Each layer represents the cross section of the part at a specific z-height. Once the data preparation is finished, the first layer of metal powder is coated on a building platform (Step 3). A laser beam passing through deflection mirrors exposes the cross

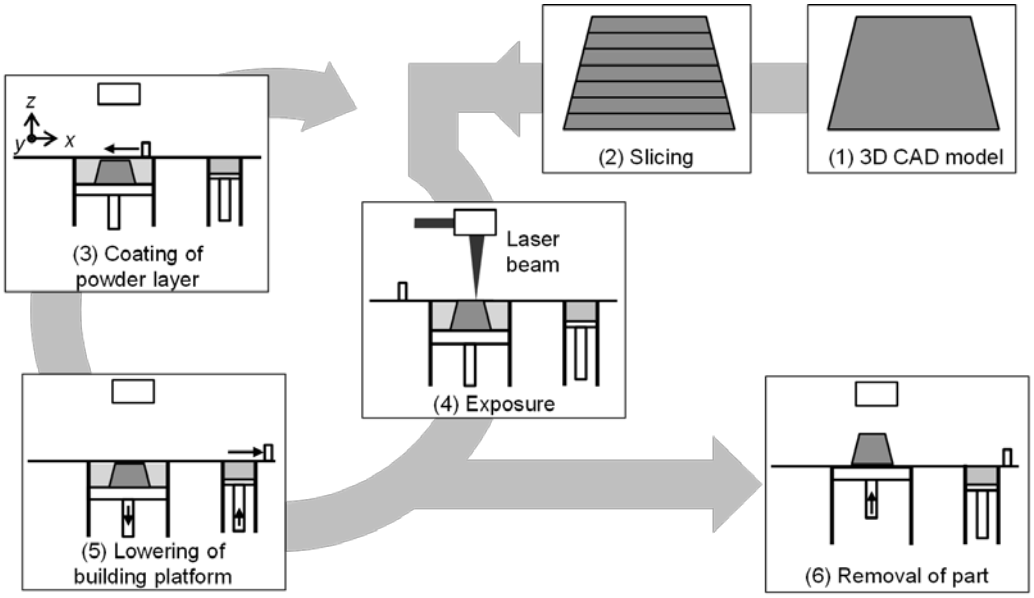

Figure 1. Process steps of SLM. The steps are numbered according to the process sequence (based on [1]).

section of the first layer (Step 4) and melts the powder material according to the slice information. The building platform is then lowered by one layer thickness (Step 5) (approx. 20-50 µm) and the next powder layer is coated. The cycle of powder coating (Step 3), laser exposure (Step 4), and platform lowering (Step 5) continues until the part is completed. The last process step is the removal of the part from the building platform (Step 6) and, if necessary, post processing.

A process has been developed to structurally integrate piezoceramic multilayer actuators (MLA) using the SLM technology. In this process the actuator is fully integrated into a metallic, monolithic SLM housing (Figure 2). Due to the layer-by-layer principle, a process interruption at a specific z-height (z_i) is required. At this point, loose metal powder is removed from the inside of the housing. The actuator is inserted into the cavity. After the insertion of the actuator, a separately manufactured cap is placed on top of the actuator to prevent loose powder trickling into the cavity. In addition, the cap functions as a plane at which the SLM manufacturing process is continued for encapsulation of the actuator.

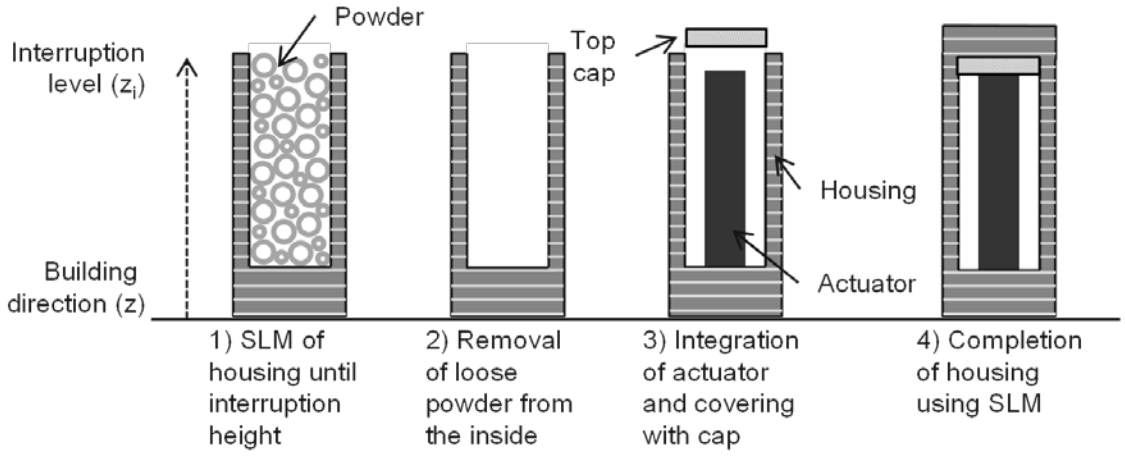

Figure 2. Process sequence for SLM of actuator modules.

For the purpose of this study the SLM housings were manufactured on an EOS M270 SLM system with a 200 W Yb-fibre laser (continuous wave, wave length λ = 1064 nm, Gaussian beam profile), using commercially available 1.4542 (17-4 PH) stainless steel powder ($d_{50} \approx 28$ µm; $d_{90} \approx 41$ µm). For all specimens, the layer thickness was fixed to 20 µm, representing the default value for the combination of material used and the SLM system. All specimens were manufactured using a meander-shaped stripe exposure which rotates along the z-axis. A qualified exposure strategy which leads to fully dense parts (laser power P = 195 W; scan speed v_s = 1000 mm/s; hatch distance h = 0.1 mm) was applied. A commercially available piezoceramic low voltage MLA (PZT material SP505) was chosen as an actuator. It is specified to create a maximum blocking force of approx. 2 kN and a maximum stroke of 45 µm. The piezoelectrically active cross section measures 49 mm². The total stack length is 32.4 mm.

Overheating of the actuator has been identified as critical since the laser-based SLM process is accompanied by high temperatures within the complete powder bed, especially in the area close to the melting zone. Previous research showed that a temperature above 200°C causes irreversible damage of the protective coating of the used MLA actuator. In an iterative development cycle the design of the housing as well as the SLM manufacturing process have been systematically adapted to avoid overheating of the actuator during completion of the housing. With adapted process parameters the maximum temperature at the actuator is approx. 180°C (Figure 3 left).

To evaluate the performance of the developed actuator modules a series of working charts were measured. The SLM generated actuator modules have been analysed in a test bench and defined voltages were applied (50 V, 100 V, 150 V, 200 V). The actuator modules were then exposed to a mechanical force by a second piezoceramic actuator inside the test bench and the elongation was measured using laser interferometers. All tests were performed with a pre-load of 100 N. Figure 3 right shows the performance charts of one actuator module for each specific driving voltage. The curves measured are almost in parallel and there is no clear difference between the slopes of each curve. Therefore, functionality of the structurally integrated piezoceramic actuator as well as mechanical coupling between housing and actuator are demonstrated.

The developed process to structurally integrate piezoceramics actuators using the SLM techniques enables the following key advantages: First, advanced reliability is achieved by protecting the actuator against non-uniaxial forces and environmental influences, particularly humidity, both of which limit

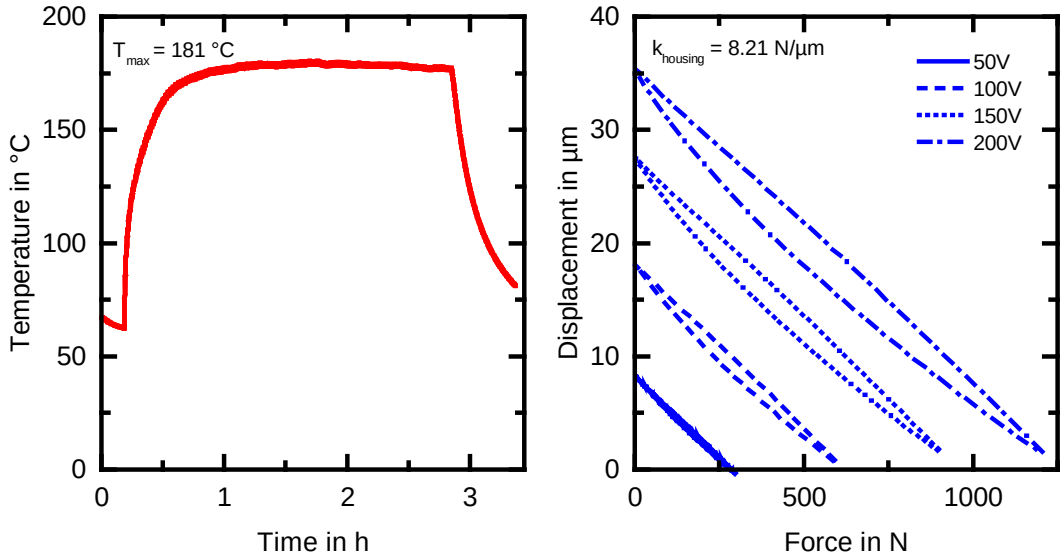

Figure 3: Temperature at the actuator during completion of the SLM housing (left). Work diagram of encapsulated MLA (right)

performance. Second, the freeform design possibility allows an application tailored design in terms of stiffness of the housing and the connection to the passive structure. A pilot implementation of the technology is an active strut for a truss structure which will be investigated in this study.

2.2 Resonant Shunt Damping with active struts

Damping of structural vibrations with passive electrical networks was already proposed by Forward [18] in 1979. The technique he presented uses piezoelectric transducers to convert the mechanical energy of a vibrating host structure into electrical energy. Since the energy is dissipated inside an electrical circuit, it is often referred as shunt damping. The most basic form of shunt damping consists of an ohmic resistor that is connected to the piezo element. That way a broadband damping effect is achieved. But the effectiveness of this technique is quite limited by the electromechanical coupling. To increase the energy transfer in a narrow frequency band, the resistive resonant shunt (RL-shunt), consisting of a resistance and an inductance is used by Forward [18]. Such an RL-shunt can be tuned to a target frequency by choosing appropriate values for the resistance and inductance. The behavior is similar to that of a mechanical vibration absorber. Since then, plenty of research has been done to describe the mathematical equations of the coupled electromechanical system and to expand the shunt circuits to more complicated ones. There exist also semi-passive and semi-active techniques. Forward [19] proposed a negative capacitance circuit to further increase the energy transfer, which would also lead to a more broadband behavior. Hagood and Crawley [6] showed first their potential for an application at space structures, which were constructed as a truss. Behrens et al., Casadei et al. and Lallart et al. [20–22] also presented implementations of shunts that are effective in broader frequency bands. Preumont et al. [23] presented the application of the resistive resonant shunt with the negative capacitance at a laboratory truss structure.

All of these techniques have in common, that their performance, either directly or indirectly, depends on the generalized electromechanical coupling coefficient. The derivation of this factor is extensively described by Hagood and Flotow [5] and its influence on the performance of a RL-shunted system is explicitly shown in [24].

Without going into the details of the shunting techniques and modelling of an electromechanically coupled structure, the following Equation (1) gives a very basic representation of the generalized electromechanical coupling coefficient K_{ij}^2

$$K_{ij}^2 = \frac{(\omega_n^D)^2 - (\omega_n^E)^2}{(\omega_n^E)^2} \tag{1}$$

In this context the variables are:

- i = index denoting the ith direction of the electrical field
- j = index denoting the jth direction of the mechanical effect
- ω_n^E = mechanical Eigenfrequency of the 1-DOF system with the piezoelectric element short circuited
- ω_n^D = mechanical Eigenfrequency of the 1-DOF system with the piezoelectric element open circuited

Equation (1) relates K_{ij} to the occurring shift of Eigenfrequency of a host structure, when the electrodes of the coupled piezo element are open or shorted. This happens due to the piezoelectric effect. The deformation induced voltage, leads in the open case to a counteractive deformation, leading to an increased stiffness of the host structure. Whereas in the closed circuit case the generated charges can flow freely and there is no electric potential. This effect is dependent on several factors, like the piezoelectric material, the stiffness of the host structure and the connection to the piezo element, its dimensions and the right position for the targeted mode. These parameters must be optimized carefully in order to achieve a satisfactory performance of the system.

3. DESIGN OF AN ACTIVE STRUT AND APPLICATION TO A TRUSS STRUCTURE

One advantage of the method of SLM is that it allows the manufacturing of customized housings for piezoelectric elements, especially for stacked actuators. In the following the numerically optimized design of an active strut in order to achieve high coupling coefficients for a given type of actuator is shown. The design is tested, when integrated into a truss structure, by using the most common type of shunt, the RL-shunt.

3.1 Numerical model of a six cell truss structure

The used test rig is a 3D truss structure with six cells, which consists of 28 nodes, which are connected through 52 short and 24 long struts. It is built as a numerical finite element model as well as a real structure (see Figure 4 and Figure 5). The truss structure is modularly constructed. The truss structure is designed as an abstraction of a bridge and comparable to other test rigs [23].

Figure 4: Truss structure (left) and installed active strut between nodes 18 and 19 (right)

The numerical finite element model is implemented with beam elements and consists of 33000 degrees of freedom (DOF). The modular image of a strut consists of the modelling of two connection bolts, two coupling nuts and the strut itself. The length of the struts is determined in the simulation model, depending on the distance between the two nods, which need to be connected.

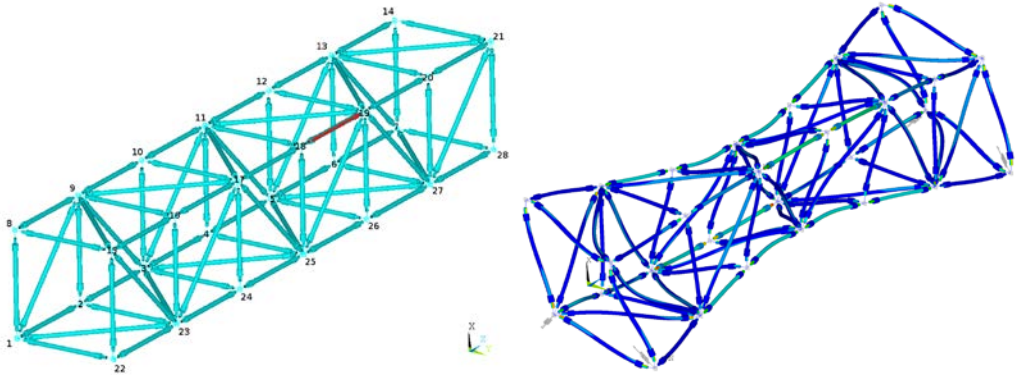

Figure 5: finite element model with active strut positioning in red (left) and elastic strain intensity in the rhombic mode 9 of the truss structure

The test rig is mounted to the bottom by weak springs at the long side of the truss structure. The 6 global modes occur till 14 Hz and can clearly be separated from the global modes. In the frequency range of 45 till 190 Hz six global modes appear. Around 50 Hz, 135 Hz, 150 Hz and 160 Hz three rhombic, the first two bending modes (in x- and y-direction) and the torsional mode appear, respectively. The modes above show local modes of the struts. The rhombic mode (mode number 9) is shown in Figure 5 (right) and the mode of interest in the following. A more detailed description of the construction of the truss structure is given in [25].

3.2 Experimental validation of the model of the truss structure

The numerical model of the truss structure is validated with the behavior of the real structure. Therefore a modal analysis of the real structure was made. The acceleration on all 28 nodes was measured using 14 Brüel & Kjaer sensors (100mV/g). The sensors were permuted during the measurement. The excitation was made with a hammer at node 13 in –x direction. The two measurements were combined to one analysis with the software LMS.testLab. Therefore the Polymax algorithm was used to determine the eigenvalues and eigenmodes. The stiffnesses of the mounts and the stiffnesses of the connection bolds were adjusted to fit the behavior of the real structure. Further the eigenvectors which contain the deformation of the eigenmodes are compared with the numerical eigenvectors. The comparison is made with the modal assurance criterion (MAC) [26] and is depicted in Figure 6. With the formula

$$MAC\left(\phi_{i,n},\phi_{j,e}\right)=\frac{\left(\phi_{i,n}^{T},\phi_{j,e}\right)^{2}}{\left(\phi_{i,n}^{T},\phi_{i,n}\right)\cdot\left(\phi_{j,e}^{T},\phi_{j,e}\right)}, \tag{2}$$

where $\phi_{i,n}$ is the i[th]-eigenvector of the numerical eigenmode and $\phi_{j,e}$ is the j[th]-eigenvector of the experimental eigenmode, the MAC values are computed.

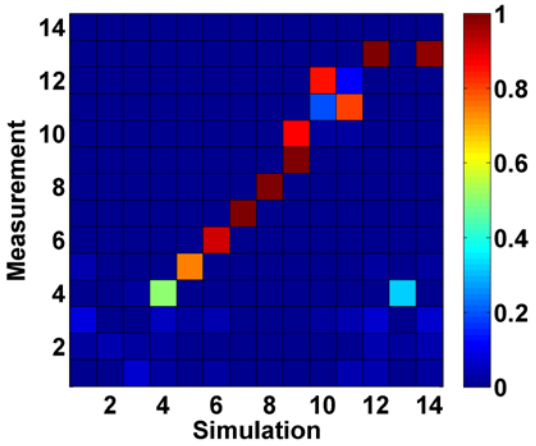

Figure 6: Result of the Modal Assurance Criterion of measured and numerical eigenmodes

A good accordance is achieved between 0.8 till 1, where the vectors are linear dependent. The eigenvectors are linear independent if the MAC values lie between 0 and 0.2. Figure 6 shows, that the rigid body modes are not clearly identified. This is caused by a sensor, which was not straight axle attached. The global modes, especially mode 9, are well identified. Clearly, the local modes, where the struts show their bending modes are not identified, since the measurement set up left local modes out.

The numerical model is fitted such that the global modes, which include mode 9, the mode of interest, are well adapted. Therefore the model can be used to determine the parameters of the shunt damping as well as positioning.

3.3 Numerical Derivation of design parameters for the active strut

The numerical investigations first consider the positioning of the active strut. Secondly, the active strut is implemented in the finite element model and at last its performance in the truss structure is shown.

The positioning to place the active strut is chosen using the elastic strain intensity of the struts. In mode 9 high elastic strain intensity occurs between nodes 18 and 19. The active strut is placed between strut 18 and 19. The coupling factors in the simulations are about 0.17 for the 10 N/µm and 0.05 for the 50 N/µm.

The active strut is implemented with a piezo stack and a parallel stiffness. The piezo stack is implemented with solid elements. The beam elements of the original struts as well as the parallel stiffness have 6 DOF. Since the solid elements used to model the piezo material have only 3 DOF, the crossover between them are solved by implementing a shell element at each end of the piezo stack.

The computation of the RL-Shunt parameters took place by the formulae

$$L = \frac{1}{\omega_E^2 C\left(1+K_{ij}^2\right)} \text{ and } R = \frac{\sqrt{2}\,K_{ij}^2}{\omega_E C(1+K_{ij}^2)}. \quad (3)$$

4. RESULTS

4.1 Experimental validation of performance of the active strut

Previous experiments showed that the stiffness of the SLM housing is below its simulated value. Reasons can be found in manufacturing imperfections which cause a divergence between designed and as-built wall thickness of the housing. The process inherent stair case effect as well as the high surface roughness of SLM parts can be argued as those imperfections. The results from the measurements in Figure 7 can be used to obtain the actual stiffness for a specific housing design (simulation).

For the purpose of this study, three different active struts were manufactures using the SLM technology. The first strut was designed to match the stiffness of a passive strut. Therefore, housing one was manufactured with a target stiffness of k_1 = 560 N/µm. In order to maximize the electromechanical coupling coefficient one housing was designed with the lowest possible target stiffness (k_2 = 10 N/µm). For the third active strut the housing stiffness was increased to k_3 = 50 N/µm to demonstrate the influence of the housing stiffness on the damping performance.

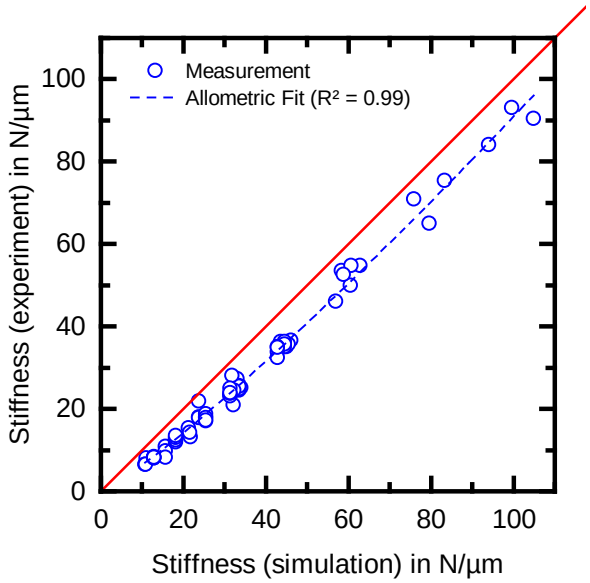

Figure 7: Comparison between experimentally determined and simulated housing stiffness.

After the manufacturing process experimental tests with the strut integrated in the truss were carried out. For that purpose, the truss was excited with an inertial mass actuator at the edge of the truss. Figure 8 shows the driving point acceleration for all three designs. With the stiffest strut the truss shows almost the same dynamic behavior as the original system and the Eigenfrequencies keep constant. Regarding this, the aim of manufacturing an active truss with an unmodified stiffness is reached. The 50 N/µm strut leads to a 4 Hz change of Eigenfrequency of mode 9 and the 10 N/µm strut to a 6 Hz change, both towards lower values.

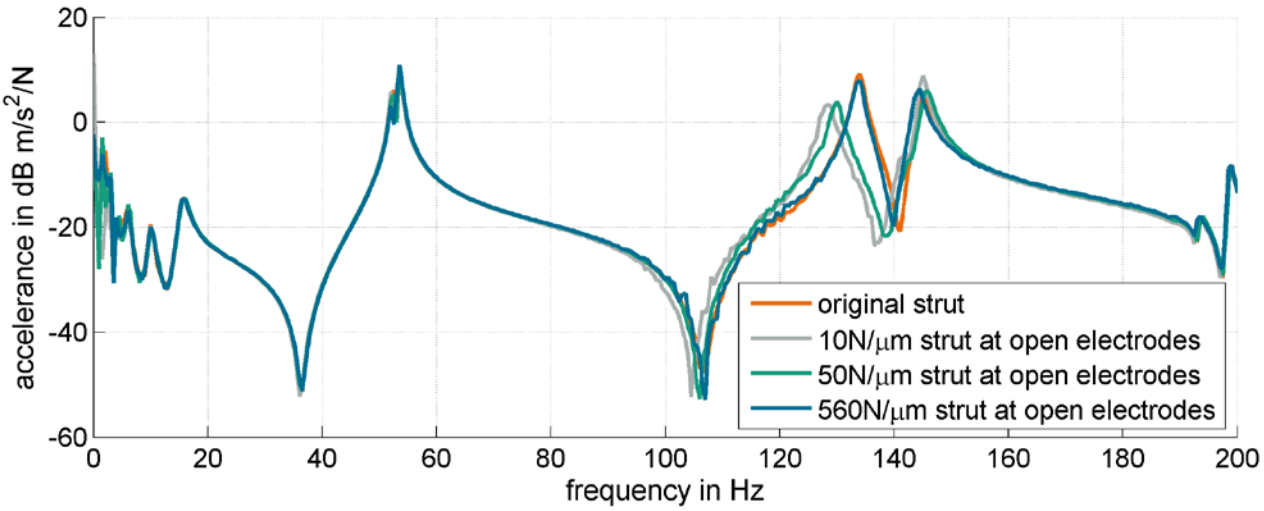

Figure 8: Driving point acceleration of the truss with different struts

An investigation of the three layouts regarding the achievable coupling coefficients, by measuring the open and short circuit Eigenfrequencies, confirms the trend of the numerically calculated values. For the stiffest strut, no coupling could be experimentally identified. The coupling coefficients can be calculated

to K_{33} = 0,126 for the 10 N/m strut and to K_{33} = 0,088 for the 50 N/µm strut. The coupling coefficient values for all struts are listed in Table 1

Table 1: Results on the coupling coefficients in the numerical simulations and the measurement

	Coupling coefficient	
stiffness	simulation	measurement
10 N/µm	0.172	0.126
50 N/µm	0.054	0.088

4.2 Experimental validation of performance of the RL-shunted truss structure

The results of the measurements indicate that the proposed design and manufacturing leads to an increased performance of the shunted system. Finally the struts were consecutively connected to an RL-shunt that was tuned to the Eigenfrequency of mode 9. Since the optimization of the shunt parameters are not focused in this paper, an experimental tuning has been done. By tuning the inductance, the two characteristic fix points, which are independent of the damping value of the shunt was equalized regarding their amplitudes. Afterwards the resistance value is increased until an optimum of vibration attenuation is achieved [27]. During the tuning process, the inductance was regularly readjusted slightly, because the next higher mode influenced the tuning at some point of the process. Figure 9 shows the resultant acceleration for the two struts with lower stiffness. Using the stiffest strut no effect could be identified. It is obvious that the 10 N/m strut achieves the highest reduction: compared to the original system the amplitude is reduced for 19.1 dB. The 50 N/µm strut achieves a vibration reduction of 16.2 dB.

The next higher mode on the other hand is in both cases slightly more excited: 3.5 dB in the case of the 10 N/m strut and 0.9 dB in the case of the 50 N/µm strut.

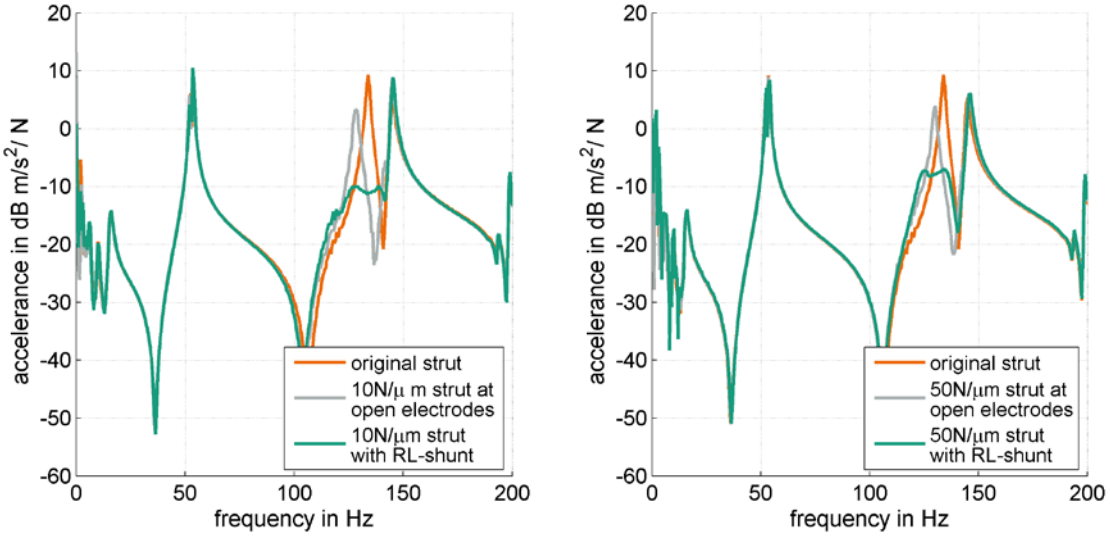

Figure 9: Driving point acceleration of the RL-shunted truss structure with a strut of 10 N/µm and of 50 N/µm stiffness

5. SUMMARY AND OUTLOOK

A scheme using selective laser melting is shown, that enables one to produce monolithically encapsulated multilayer actuators. The proposed technology allows the manufacturing of application tailored actuator modules (e.g. stiffness, connection to passive structure) with a reliable protection against harming environmental influences (e.g. humidity, shear forces).

The validated simulation model of the truss structure can be used to dimension specific parameters, like the housing stiffness and actuator dimensions. Three active struts were manufactured using the SLM technology. It is shown, that application specific designs can be produced, which influence the dynamic behavior of the truss structure. One strut has the same stiffness than the original struts. Two further struts have lower stiffnesses of 10N/µm and 50N/µm. There the coupling coefficient K_{33} is optimized to be large. The reduction in mode 9 of the application truss structure is 16,2dB till 19,1dB, respectively.

Further work will be investigated into negative capacitance to increase the shunting effect. Furthermore the reliability of the monolithically designed smart devices will be investigated.

ACKNOWLEDGMENTS

This research work was funded by the LOEWE Research Center AdRIA (Adaptronic Research, Innovation, Application) grant number III L 4 – 518/14.0004 (2008). The authors would like to thank the Hessen State Ministry of Higher Education, Research and the Arts for its support. The authors would also like to thank David Flaschenträger and Sebastian Sprengart for preparatory work.

REFERENCES

1. Poprawe, R., *Lasertechnik für die Fertigung. Grundlagen, Perspektiven und Beispiele für den innovativen Ingenieur*, Springer, Berlin [u.a.], 2005.
2. Juang, J.-N., "Optimal design of a passive vibration absorber for a truss beam," *Journal of Guidance, Control, and Dynamics*; Vol. 7, No. 6, 1984, pp. 733–739.
3. Cohen, K., and Weller, T., "Passive Damping Augmentation For Vibration Suppression In Flexible Latticed Beam-like Space Structures," *Journal of Sound and Vibration*; Vol. 175, No. 3, 1994, pp. 333–346.
4. Matunaga, S., Yu, Y., and Ohkami, Y., "Vibration Suppression Using Acceleration Feedback Control with Multiple Proof-Mass Actuators," *AIAA Journal*; Vol. 35, No. 5, 1997, pp. 856–862.
5. Hagood, N. W., and Flotow, A. von, "Damping of structural vibrations with piezoelectric materials and passive electrical networks," *Journal of Sound and Vibration*; Vol. 146, No. 2, 1991, pp. 243–268.
6. Hagood, N. W., and Crawley, E. F., "Experimental investigation into passive damping enhancement for space structures," *Journal of Guidance, Control, and Dynamics*; Vol. 14, No. 6, 1991, pp. 1100–1109.
7. Schütze, R., Goetting, H., Breitbach, E., and Grützmacher, T., "Lightweight engine mounting based on adaptive CFRP struts for active vibration suppression," *Aerospace Science and Technology*; Vol. 2, No. 6, 1998, pp. 381–390.
8. Crawley, E. F., and Luis, J. de, "Use of piezoelectric actuators as elements of intelligent structures," *AIAA Journal*; Vol. 25, No. 10, 1987, pp. 1373–1385.

9. Mayer, D., Melz, T., Pille, C., and Wöstmann, F. J., "CASTTRONICS - Direct integration of piezo ceramic materials in high pressure die casting parts for vibration control," *ACTUATOR 2008, 11th International Conference on New Actuators, Bremen, Germany, 9.-11.6.2008*, 2008.
10. Schubert, A., Wittstock, V., Koriath, H.-J., Jahn, S. F., Peter, S., Müller, B., and Müller, M., "Smart metal sheets by direct functional integration of piezoceramic fibers in microformed structures," *Microsystem Technologies*; Vol. 20, No. 6, 2014, pp. 1131–1140.
11. Gibson, I., Rosen, D. W., and Stucker, B., *Additive manufacturing technologies. Rapid prototyping to direct digital manufacturing*, Springer, New York, NY, 2010.
12. Huang, S. H., Liu, P., Mokasdar, A., and Hou, L., "Additive manufacturing and its societal impact: a literature review," *The International Journal of Advanced Manufacturing Technology*; Vol. 67, 5-8, 2013, pp. 1191–1203.
13. Zhai, Y., Lados, D. A., and LaGoy, J. L., "Additive Manufacturing: Making Imagination the Major Limitation," *JOM*; Vol. 66, No. 5, 2014, pp. 808–816.
14. Gu, D. D., Meiners, W., Wissenbach, K., and Poprawe, R., "Laser additive manufacturing of metallic components: materials, processes and mechanisms," *International Materials Reviews*; Vol. 57, No. 3, 2012, pp. 133–164.
15. Grzesiak, A., Becker, R., and Verl, A., "The Bionic Handling Assistant: a success story of additive manufacturing," *Assembly Automation*; Vol. 31, No. 4, 2011, pp. 329–333.
16. Petrovic, V., Vicente Haro Gonzalez, Juan, Jordá Ferrando, O., Delgado Gordillo, J., Ramón Blasco Puchades, Jose, and Portolés Griñan, L., "Additive layered manufacturing: sectors of industrial application shown through case studies," *International Journal of Production Research*; Vol. 49, No. 4, 2011, pp. 1061–1079.
17. Campbell, I., Bourell, D., and Gibson, I., "Additive manufacturing: rapid prototyping comes of age," *Rapid prototyping journal*; Vol. 18, No. 4, 2012, pp. 255–258.
18. Forward, R. L., "Electronic damping of vibrations in optical structures," *Applied optics*; Vol. 18, No. 5, 1979, pp. 690–697.
19. Forward, R. L., *Electromechanical transducer-coupled mechanical structure with negative capacitance compensation circuit*, 1979.
20. Behrens, S., Fleming, A. J., and Moheimani, S O R, "A broadband controller for shunt piezoelectric damping of structural vibration," *Smart Materials and Structures*; Vol. 12, No. 1, 2003, pp. 18–28.
21. Casadei, F., Ruzzene, M., Dozio, L., and Cunefare, K. A., "Broadband vibration control through periodic arrays of resonant shunts: experimental investigation on plates," *Smart Materials and Structures*; Vol. 19, No. 1, 2010, p. 015002.
22. Lallart, M., Harari, S., Petit, L., Guyomar, D., Richard, T., Richard, C., and Gaudiller, L., "Blind switch damping (BSD): A self-adaptive semi-active damping technique," *Journal of Sound and Vibration*; Vol. 328, 1-2, 2009, pp. 29–41.
23. Preumont, A., Marneffe, B. de, Deraemaeker, A., and Bossens, F., "The damping of a truss structure with a piezoelectric transducer," *Computers & Structures*; Vol. 86, 3-5, 2008, pp. 227–239.
24. Hollkamp, J. J., and Starchville, T. F., "A Self-Tuning Piezoelectric Vibration Absorber," *Journal of Intelligent Material Systems and Structures*; Vol. 5, No. 4, 1994, pp. 559–566.
25. Flaschenträger, D., Thiel, J., Rausch, J., Atzrodt, H., Herold, S., Melz, T., Werthschützky, R., and Hanselka, H., "Implementation and Characterisation of the Dynamic Behaviour of a Three-dimensional Truss Structure for Evaluating Smart Devices," *ISMA 2010, 24th International Conference on Noise and Vibration Engineering, Leuven, Belgium, 20.-22.9.2010*, 2010.
26. Ewins, D. J., *Modal testing. Theory, practice, and application*, 2nd edn., Research Studies Press, Baldock, Hertfordshire, England, Philadelphia, PA, 2000.
27. Tang, J., and Wang, K. W., "Active-passive hybrid piezoelectric networks for vibration control: comparisons and improvement," *Smart Materials and Structures*; Vol. 10, No. 4, 2001, pp. 794–806.